J. Fluid Mech. (1985), *vol.* 161, *pp.* 347–369
Printed in Great Britain

The effect of convex surface curvature on turbulent boundary layers

By K. C. MUCK†, P. H. HOFFMANN‡ AND P. BRADSHAW
Department of Aeronautics, Imperial College, London

(Received 24 April 1984 and in revised form 8 July 1985)

The response of a well-developed turbulent boundary layer to suddenly applied convex surface curvature is investigated, using conditional-sampling techniques so that the turbulent and non-turbulent regions of the flow can be clearly distinguished. The conclusion of this and the companion paper by Hoffmann, Muck & Bradshaw (1985) is that the effects of convex (stabilizing) and concave (destabilizing) curvature on boundary layers – and presumably on other shear layers – are totally different, even qualitatively: mild convex curvature, with a radius of curvature of the order of 100 times the boundary-layer thickness, tends to attenuate the pre-existing turbulence, apparently without producing large changes in statistical-average eddy shape, while concave curvature results in the quasi-inviscid generation of longitudinal ('Taylor–Görtler') vortices, together with significant changes in the turbulence structure induced directly by the curvature and indirectly by the vortices.

From the point of view of calculation methods, the implication is that, although stabilizing and destabilizing curvature are connected by a common dimensional analysis, the differences are such that the one cannot be regarded as a useful guide to the treatment of the other. Specifically, rates of change of turbulence-structure parameters with curvature parameter are likely to be nearly discontinuous at zero curvature, and in particular the time of response of a turbulent boundary layer to convex curvature, implying mere attenuation, is very much less than the time of response to concave curvature, implying reorganization of the eddy structure.

1 Introduction

The paper is one of a series on complex turbulent flows (defined as shear layers with complicating influences like distortion by an extra rate of strain or interaction with another turbulence field). A previous paper on curvature in the series is that of Smits, Young & Bradshaw (1979) describing an experiment on strongly curved boundary layers, which was conceived at a time when it was believed that the effects of mild surface curvature on boundary layers were relatively well understood. The present paper is a continuation of the work of Meroney & Bradshaw (1975), and uses the same test rig in which a well-developed low-speed turbulent boundary layer encounters a longitudinally curved surface with a radius of curvature about 100 times the initial thickness of the boundary layer. That is, the boundary layer is perturbed by a step increase in curvature, as distinct from the 'impulse' of curvature (i.e. a sharp bend) in the experiment of Smits *et al.*; the total turning angle in the present

† Present address: Research Division, United Technologies – Carrier Corp., Syracuse, NY 13221, USA.
‡ Present address: Department of Civil and Aero Engng, Royal Melbourne Inst. of Tech., Melbourne, Vic. 3000, Australia.

experiment (see figure 1) is roughly the same as in the sharp-bend experiment. As in the work of Meroney & Bradshaw and of Smits *et al.*, we have considered both convex and concave curvature, and perhaps our most important conclusion, based upon our own work and that of others, is that there is practically no useful connection between the two cases. We have signalized this by presenting the work in two papers, the work of Hoffmann, Muck & Bradshaw (1985) on concave curvature being referred to hereinafter as II. The implication is that allowances for the effect of streamline curvature in calculation methods for turbulent flow should be formulated separately for the stabilizing and destabilizing cases. The same conclusion appears to apply to the stabilizing and destabilizing effects of body forces such as buoyancy: empirical correlations in the meteorological literature are usually algebraically different for each sign of buoyancy. (The simpler formulae even have discontinuities of slope at zero buoyancy parameter.) The effects of 'stabilizing' and 'destabilizing' curvature on laminar flows are of course totally different: stabilizing curvature has a small, $O(\delta/R)$, effect on Tollmien–Schlichting waves, while destabilizing curvature leads to a new instability mode, Taylor–Görtler vortices.

It is well known that the effects of streamline curvature or other 'extra rates of strain' on turbulent shear layers are an order of magnitude larger than would appear from the explicit metric terms which appear when the mean-flow and turbulence transport equations are written in the semi-curvilinear coordinates appropriate to distorted shear layers. The computations presented at the 1980–81 Stanford meeting on Complex Turbulent Flows (Kline, Cantwell & Lilley 1982) showed that, contrary to some previous claims, none of the calculation methods was capable of reproducing the effects of streamline curvature without the introduction of explicit correction terms. The two-point-correlation method of Jeandel *et al.* (see Kline *et al.*, vols. 2 and 3) may be an exception, but it was tested only for the allied case of rotation in a homogeneous turbulent flow. Kline (see Kline *et al.*) has strongly argued that it is neither immoral, nor necessarily imprudent, to allow the empirical coefficients in a turbulence model to depend upon the type of flow being calculated, providing that the flow-identification process and the behaviour of the coefficients can be specified beforehand (i.e. in a computer program) so that intervention by the user of the calculation method is not required. (Adjustment of quantitative parameters according to results of qualitative or semi-quantitative pattern recognition – in the broadest sense of the latter term – is the basis of so-called 'expert systems'.) Here we need to consider only a mild version of the principle of 'zonal modelling', requiring some of the empirical functions or coefficients in a turbulence model to depend on the sign of the curvature. Although the present results refer specifically to turbulent boundary layers, it is probable that similar arguments would apply qualitatively to other curved shear layers.

Curved shear layers may exhibit near-equilibrium behaviour if the ratio of shear-layer thickness to streamline curvature is independent of downstream distance, but the non-equilibrium state, of which an extreme example is suddenly applied curvature, is equally important in practice. This introduces the time of response of a turbulent flow to surface curvature, as well as the asymptotic magnitude of response. At the phenomenological level, the most spectacular difference between the response of a turbulent boundary layer to a concave curvature and a convex curvature is that in the latter case the response is much more rapid, as is shown by a comparison of the present results with those of II. A general review of curvature effects was given recently in this journal by Gillis & Johnston (1983).

Several other workers (e.g. So & Mellor 1973; Ramaprian & Shivaprasad 1978;

Gillis *et al.* 1980; Gillis & Johnston 1983) have reported measurements of the Reynolds stresses in convex-curved boundary layers. Ramaprian & Shivaprasad measured triple products, but used nonlinearized constant-current hot wires so that the results are not reliable; and at the time that the present work was started the only experiment that included triple-product measurements, so that all the terms in the Reynolds-stress transport equation could be deduced, was the work of Castro & Bradshaw (1976) on a stably curved mixing layer with a very short region of curvature. More recently, Gibson, Verriopoulos & Vlachos (1984) have measured velocity and temperature-fluctuation statistics up to third order in a rig similar to the present one. It seemed appropriate to extend the work of Meroney & Bradshaw to include triple-product measurements and conditional sampling, in order to provide comprehensive documentation of a mildly curved boundary layer in which the stabilizing effects of curvature significantly attenuate the turbulence, but are not strong enough to annihilate the shear stress in the outer part of the layer as found in some of the strongly curved experiments. The measurements were not aimed at the improvement of any particular calculation method, or even a class of calculation methods, but the paper includes a discussion of the implications for turbulence modelling in general.

2. Apparatus and techniques

The measurements were made in the blower tunnel rig used by Meroney & Bradshaw (1975), shown in figure 1 (*a*). The convex surface has a radius of curvature of 2410 mm. The working section was 762 mm wide and 127 mm high: the flow speed at the start of the working section was about 33 m s^{-1}, and increased slightly down the length of the working section owing to boundary layer growth. The surface-pressure coefficient, referred to conditions at the working-section entrance, is shown in figure 1 (*b*). The free-stream turbulence level at the working-section entrance was about 0.1%. A 0.7 mm diameter trip wire was installed on each surface at the working-section entrance. The boundary-layer thickness at the start of the curved section is about 22 mm ($U_e \theta/\nu = 5000$, $\delta/R = 0.009$), increasing to about 33 mm at exit on the convex side and about 45 mm on the concave side: that is, the thickness of the free-stream core was always at least 1.5 times the thickness of the convex-surface boundary layer, and the ratio of tunnel width to convex-surface boundary-layer thickness was always at least 20. There is a short region of fairly strong pressure gradient at the start of curvature but, unlike Gillis & Johnston, we made no attempt to eliminate this transient effect or the slight favourable pressure gradient down the working-section length as a whole, because (i) the effects of small mean-pressure gradients are fairly well understood and are quite easily accounted for in most calculation methods, and (ii) the mean-pressure gradients do not appear explicitly in the transport equations for the Reynolds stresses, so that any effects of pressure gradient on the Reynolds stresses are indirect.

Mean velocities were measured with conventional Pitot tubes, being deduced from the pressure difference between the Pitot tube and the wall static-pressure tapping by the method of So & Mellor (1972), which assumes that the normal pressure gradient is equal to $\rho U^2/(y+R)$, where U is the local mean velocity and R is the radius of curvature of the surface. Use of surface curvature rather than local streamline curvature is consistent with the customary neglect of normal pressure gradient in a boundary layer on a flat surface. No attempt was made to measure static pressure within the stream, because of the large effects of turbulence on static-pressure probes

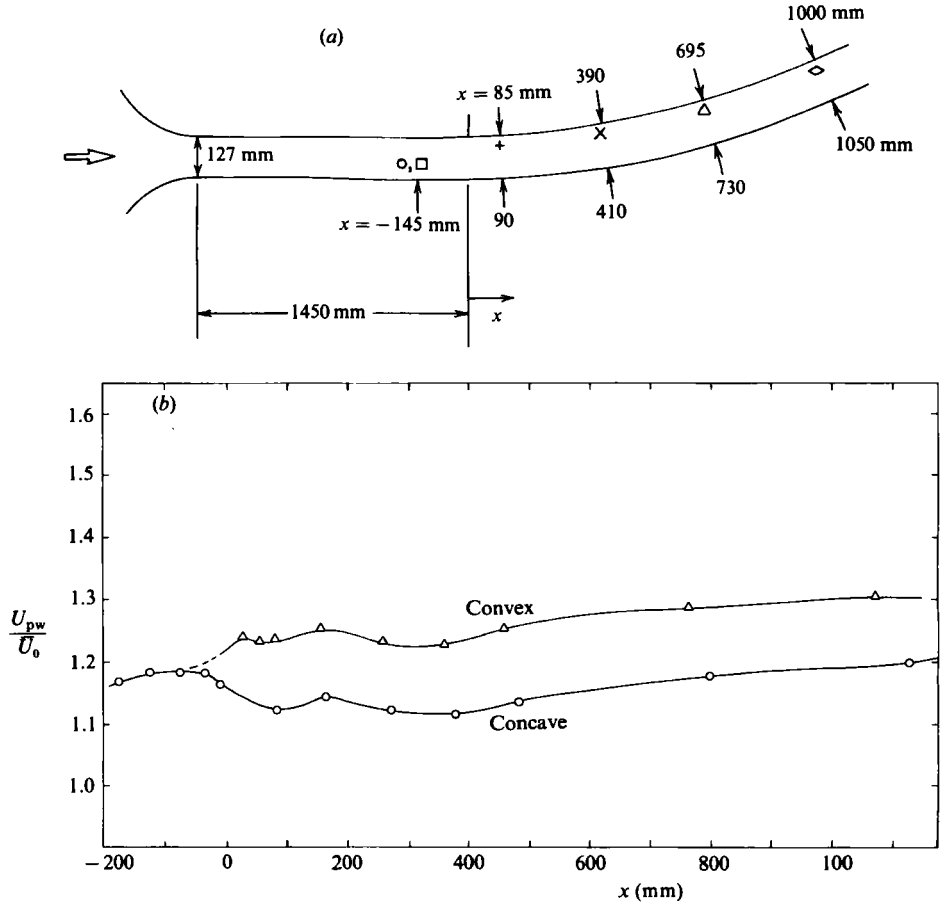

FIGURE 1. Experimental arrangement. (*a*) Side view of test section, showing symbols for figures 5–14. Curvature starts at $x = 0$; width 762 mm, convex-wall radius 2410 mm. (*b*) Streamwise distribution of the wall static pressure: U_{pw} is 'potential velocity at wall' defined by $(p-p_0)/\frac{1}{2}\rho U_0^2 = 1-(U_{pw}/U_0)^2$.

(Christiansen & Bradshaw 1981). Given the static pressure, we can define a pseudo-potential-flow velocity U_p by $\frac{1}{2}\rho U_p^2 = P_e - p$, where P_e is the free-stream total pressure. The customary definitions of displacement and momentum thickness for a curved surface result from replacing the usual free-stream velocity U_e by U_p in the definition, and the simplest definition of skin-friction coefficient is in terms of the value of U_p at the surface, U_{pw}. Alternatively the velocity can be based on surface static pressure and measured total pressure. The differences are small, and the latter definition should be consistent with a prediction method that ignores normal pressure gradients and accepts the surface static pressure as the input. Surface shear stress was deduced from Preston-tube readings, and, equivalently, by fitting a portion of the mean-velocity profiles to the logarithmic law of the wall.

Hot-wire measurements were made with constant-temperature DISA 55D01 anemometers, with 5 μm diameter platinum wires soldered on to Prosser 6525 X-probes. Temperature fluctuations were measured, solely for intermittency measurement, with 1 μm diameter platinum wires, operated at a constant current of about 1 mA and compensated for thermal inertia by a home-made amplifier circuit.

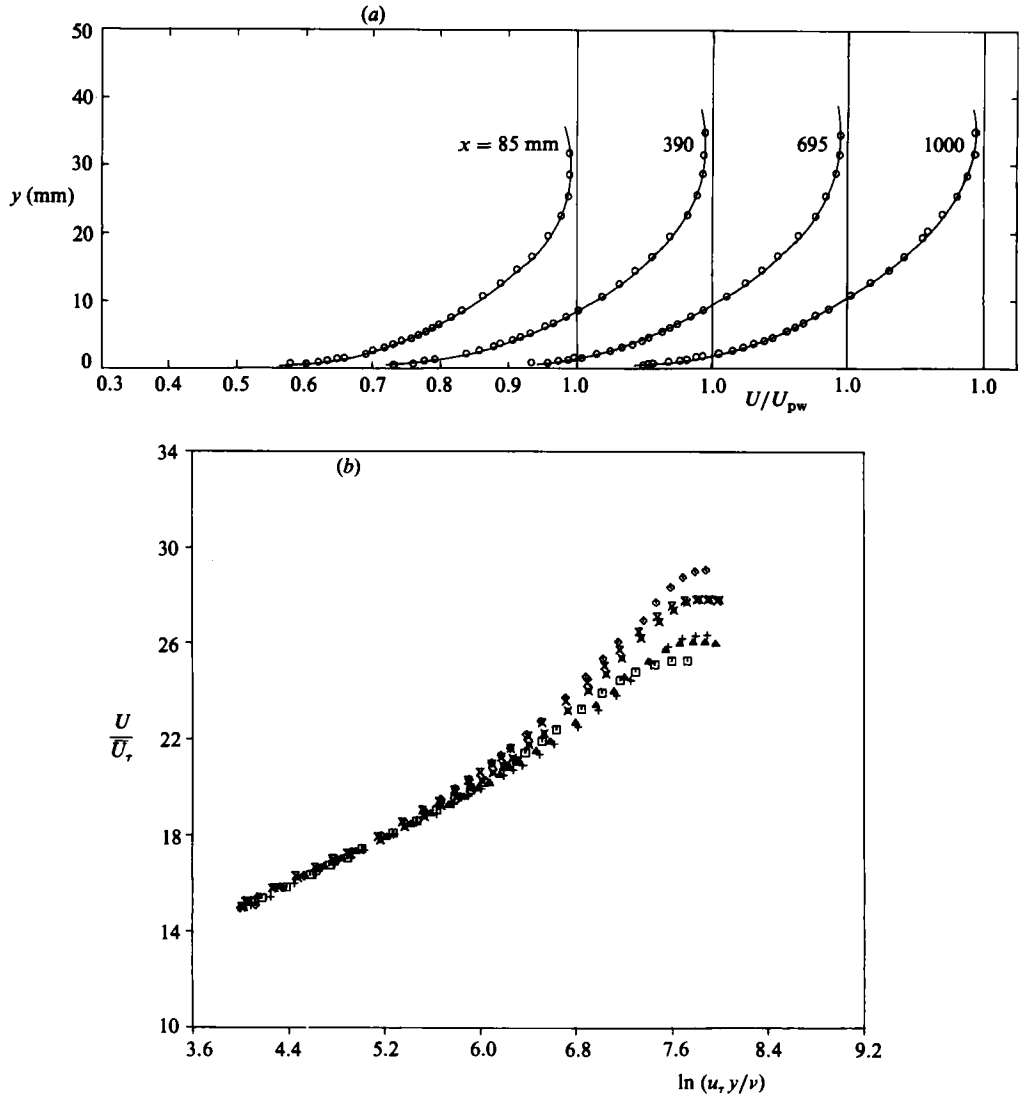

FIGURE 2. Mean-velocity profiles. (*a*) Linear scales. (*b*) Semilogarithmic scales: straight line is logarithmic law for plane flow, $U/u_\tau = (1/0.41)\ln(u_\tau y/\nu)+5.2$. □, +, $x = -145$ mm, $c_{f,\,\max}$ and $c_{f,\,\min}$; △, 85; ⧖, 390; ⧈, 695; ◇, 1050.

Resistance-thermometer compensation was set by observing the output trace in an intermittently hot region of the flow, and adjusting the electronics so that, at the end of a hot 'burst', the temperature decreased to the 'cold' level as rapidly as possible without overshoot. For more details of the techniques and the intermittency algorithm see Weir, Wood & Bradshaw (1981). Heat was introduced into the boundary layer by means of heated wires near the roof and floor of the settling chamber of the wind tunnel, the thermal wakes of the wires being entrained into the boundary layers quite close to the start of the working section. Temperature differences within the boundary layer were between 1.5 and 3 °C.

Fluctuating signals from probes carrying two cross wires and one temperature wire were recorded simultaneously on analog magnetic tape, and later transcribed to

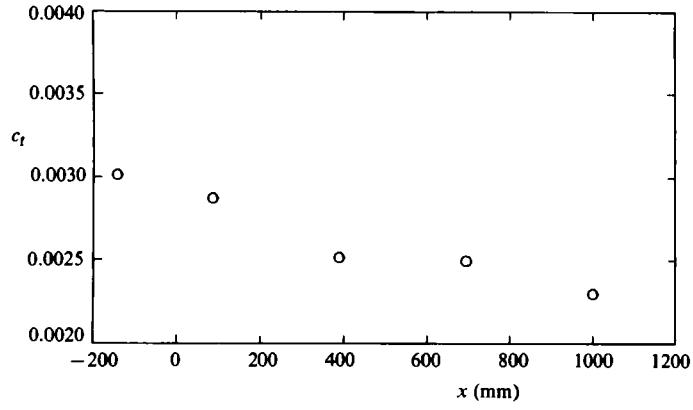

FIGURE 3. Skin-friction coefficient, $c_f = \tau_w/\frac{1}{2}\rho U_{pw}^2$.

digital magnetic tape for processing on the College computer. Overall frequency response was at least 10 kHz. The data-analysis program allowed for the effect of temperature fluctuation on the velocity signal, the effect of velocity fluctuations on the temperature wire being negligible.

Details of the measurement techniques in general, and of calibration techniques and precautions to reduce errors in particular, are given by Muck (1982); microfiche copies of this thesis, and magnetic tapes of the data, are available from Imperial College. The experiment is not an especially demanding one as far as hot-wire techniques are concerned, and the general accuracy is demonstrated by the agreement of pre-curvature results – for, say, R_{uv} (figure 5*e*) – with existing data. Absolute accuracy is probably of the order usually attainable in hot-wire measurements, i.e. better than 10% for Reynolds stresses, better than 15% for triple products.

3. Results

The measurement positions on the convex and concave surfaces (figure 1*a*) are on the same radial lines, but necessarily at different values of x measured along each surface from the start of the curvature. Only a selection of the results is given here, as a support for the discussion. For details see Muck (1982).

Figure 1 (*b*) shows the pressure distributions on the convex and concave surfaces: note that $(U_{pw}/U_0)^2$, where U_0 is the speed at entrance to the working section, equals $1-c_p$ with c_p based on $\frac{1}{2}\rho U_0^2$. Pressure gradients are small except near the start of curvature. The mean-velocity profiles are plotted as true U/U_{pw} in figure 2: $c_{f,max}$ and $c_{f,min}$ refer to different spanwise stations on the concave surface (see II). The profiles plotted in semilogarithmic form in figure 2 (*b*) follow the universal logarithmic law accurately at small y, but then diverge from it at a value of y which decreases with increasing downstream distance. This is an immediate indication of the rather slow response of the boundary layer to the sudden imposition of curvature: recall that R is constant, while u_τ decreases only slowly with increasing x, so that any curvature parameter based on inner-layer variables also changes only slowly with x. This does not necessarily imply slow response of small-scale inner-layer turbulence, because the point at which the velocity profile leaves the logarithmic law depends on the *outer*-layer turbulence. The mean-velocity profiles do follow the logarithmic law in slope (whereas the deduction of u_τ from a log-law fit merely requires the

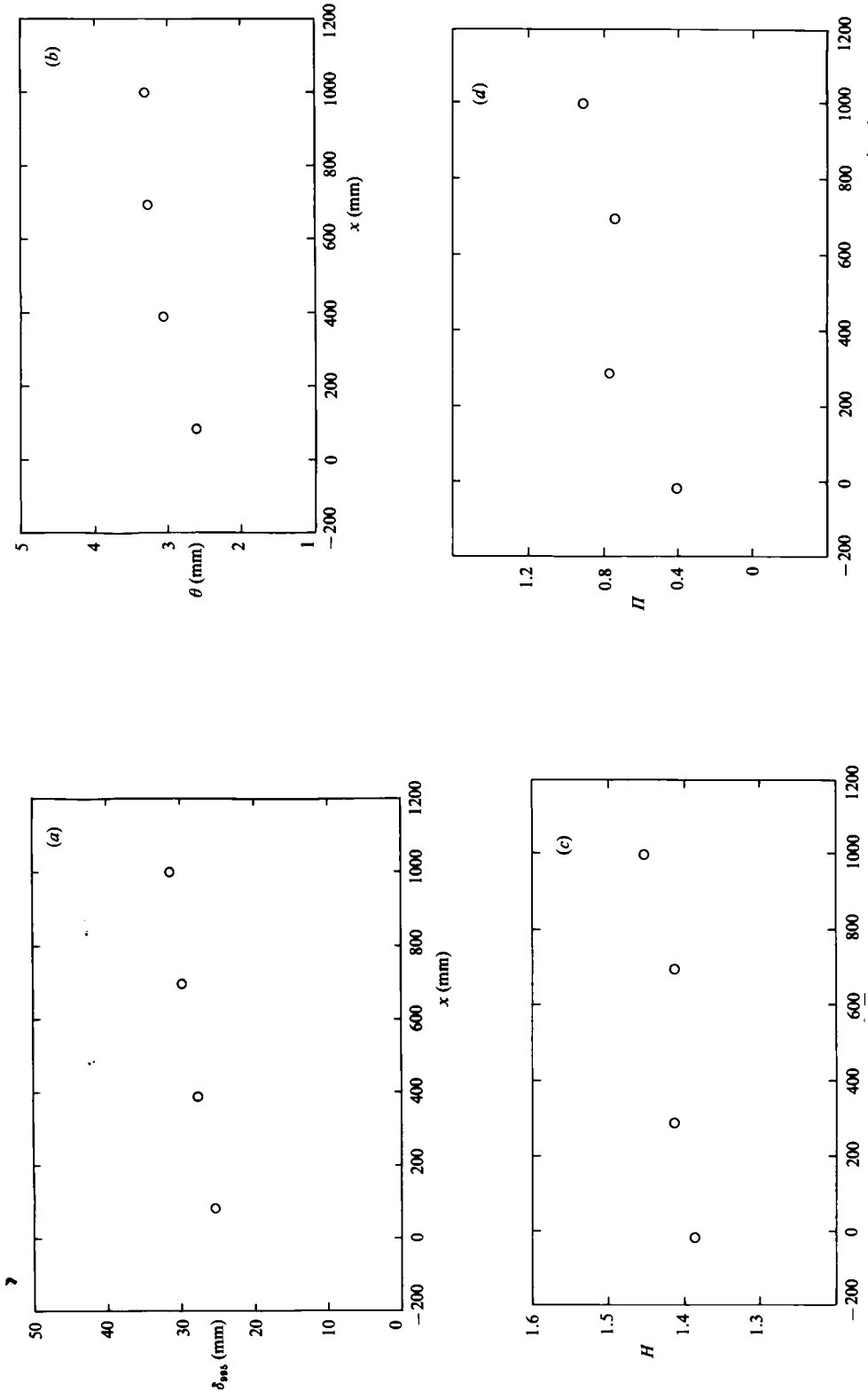

FIGURE 4. Velocity-profile parameters. (*a*) Boundary-layer thickness. (*b*) Momentum thickness. (*c*) Shape factor H. (*d*) Wake parameter Π.

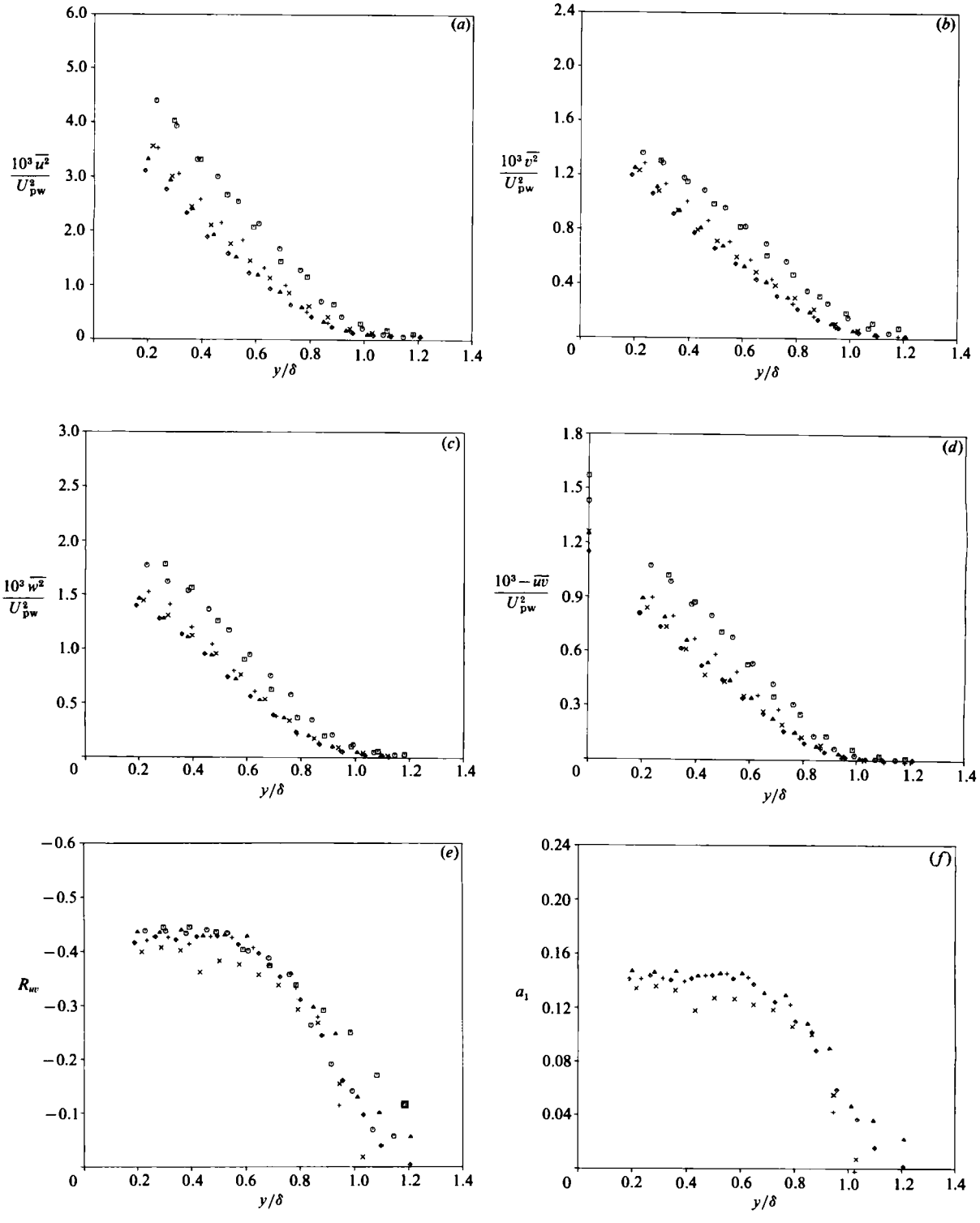

FIGURE 5. Profiles of the Reynolds stresses: see figure 1 (*a*) for symbols. (*a*) $10^3\overline{u^2}/U_{pw}^2$. (*b*) $10^3\overline{v^2}/U_{pw}^2$. (*c*) $10^3\,\overline{w^2}/U_{pw}^2$. (*d*) $10^3(-\overline{uv}.U_{pw}^2$. (*e*) Shear-stress correlation coefficient $R_{uv} = (-\overline{uv})/(\overline{u^2}\,\overline{v^2})^{\frac{1}{2}}$. (*f*) $a_1 = -\overline{uv}/(\overline{u^2}+\overline{v^2}+\overline{w^2})$.

measured profile to intersect the universal profile *somewhere*). This supports the intuitive feeling that if y/R, and therefore the ratio of eddy size to R, is small enough the effects of curvature on the turbulence structure will be negligibly small. The skin-friction coefficient, based on the surface value of the potential-flow velocity U_p defined above, is shown in figure 3, and the boundary-layer thickness, defined as the distance from the surface at which the velocity is 0.995 of the potential-flow velocity, is shown in figure 4(*a*). Expected values for constant-pressure boundary layers on flat surfaces are given by the approximate formula $c_f = 0.026\ (U_e\theta/\nu)^{-\frac{1}{4}}$, which gives $c_f = 0.0028$ at the last station, compared to 0.0023. Figure 4 also shows the momentum thickness θ, the shape factor $H = \delta^*/\theta$ and the 'wake parameter' Π, at slightly different values of x from c_f and δ_{995}. Here Π is defined in terms of the divergence from the universal law of the wall, without any curved-surface correction. Insertion of measured quantities into the two-dimensional momentum-integral equation shows a small imbalance, less than 10% of the c_f term, which is attributable to lateral divergence (the discrepancy is in the wrong sense to be explained by secondary flow near the sidewalls, which in any case appears to be small). This imbalance might need to be taken into account in comparison with calculations of mean-flow quantities but is far too small to affect turbulence-structure parameters.

Reynolds stresses are shown in figure 5. In all cases, the stress decreases rather rapidly from the pre-curvature station to the station 85 mm (about 4δ) after the start of the curvature, and thereafter decreases more slowly, roughly following the slow decrease of surface shear stress. Our results differ noticeably from those of Gibson *et al.* The discrepancy at the pre-curvature stations is mainly in $\overline{w^2}$: their results agree fairly closely with the classical measurements of Klebanoff (1955) whereas ours show the smaller difference between $\overline{v^2}$ and $\overline{w^2}$ found in most of the more recent experiments. At later stations the results diverge further, because our δ/R was rather larger than theirs. (The simplest parameter to quote is the ratio of x to R at the start of the curvature: 0.5 in the work of Gibson *et al.*, 0.6 in ours.) Note that δ/R, or any other curvature parameter, increases slowly with x, so the results imply that equilibrium with the *local* curvature is achieved by about 4δ after the start of curvature: for a further discussion of response times see paper II. The most noteworthy feature of the response to convex curvature is the increase in $\overline{u^2}$, relative to the other intensity components, near the outer edge, accompanied by a slight relative *decrease* in $\overline{u^2}$ in the main part of the boundary layer. The ratios are plotted by Muck: the trend in $\overline{v^2}/\overline{u^2}$ is similar to that of Gibson *et al.* and somewhat less pronounced than in Gillis & Johnston's experiment, and the small decrease near the outer edge is in contrast with the large increases found in the concave case in paper II. The shear correlation coefficient and the stress/intensity ratio, figure 5(*e*, *f*), are barely reduced by curvature, except for a significant decrease in the outer part of the boundary layer. Here the results agree fairly closely with those of Gibson *et al.*: their plateau value of R_{uv} on a flat surface is about 0.47 while ours is about 0.43, the usual textbook/consensus value being 0.45. This suggests that the two experiments are reasonably consistent and that the differences in the measured intensities are mostly the effect of differences in curvature parameter.

Figure 6 shows the effect of streamline curvature on the mixing length and eddy viscosity, non-dimensionalized by δ_{995} and $U_{pw}\delta^*$ respectively, as usual. It must be remembered that the mixing length and eddy viscosity are not turbulence parameters, but ratios of turbulence quantities to the mean-flow quantity $\partial U/\partial y$: therefore the decrease in mixing length after the application of curvature is attributable partly to the decrease in shear stress shown in figure 5 and partly to the increase in $\partial U/\partial y$ shown

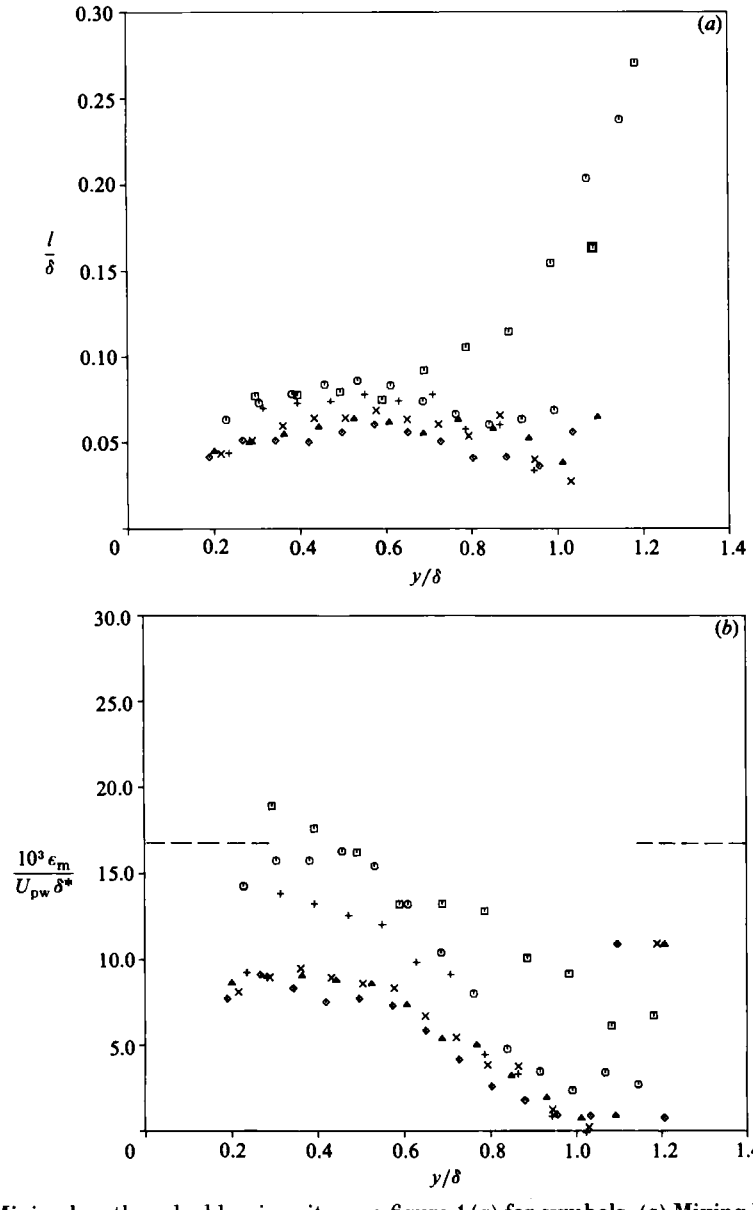

FIGURE 6. Mixing length and eddy viscosity: see figure 1 (*a*) for symbols. (*a*) Mixing length l_m/δ_{995}. (*b*) Eddy viscosity $10^3\epsilon_m/(U_{pw}\delta^*)$: dotted line shows 'standard' value $\epsilon_m = 0.0168U_e\delta^*$.

in figure 2. The reductions in mixing length and eddy viscosity are largest in the outer part of the boundary layer, and the streamwise development is again virtually complete by the third measuring station, at $x = 390$ mm about 15δ from the start of curvature. It is not very useful to correlate the results in terms of local-curvature parameter – as shown by Muck, the 'Richardson number' changes very little once the curvature is established – but a typical Richardson number at $y/\delta = 0.5$ is about 0.03, and the observed reduction in $1/\delta$ to about 0.65 of its upstream value at this y/δ corresponds to the usual factor of 10 connecting curvature parameter and shear-stress response. The fractional decrease in mixing length found by Gibson *et al.* is slightly less, their curvature parameters being slightly less also.

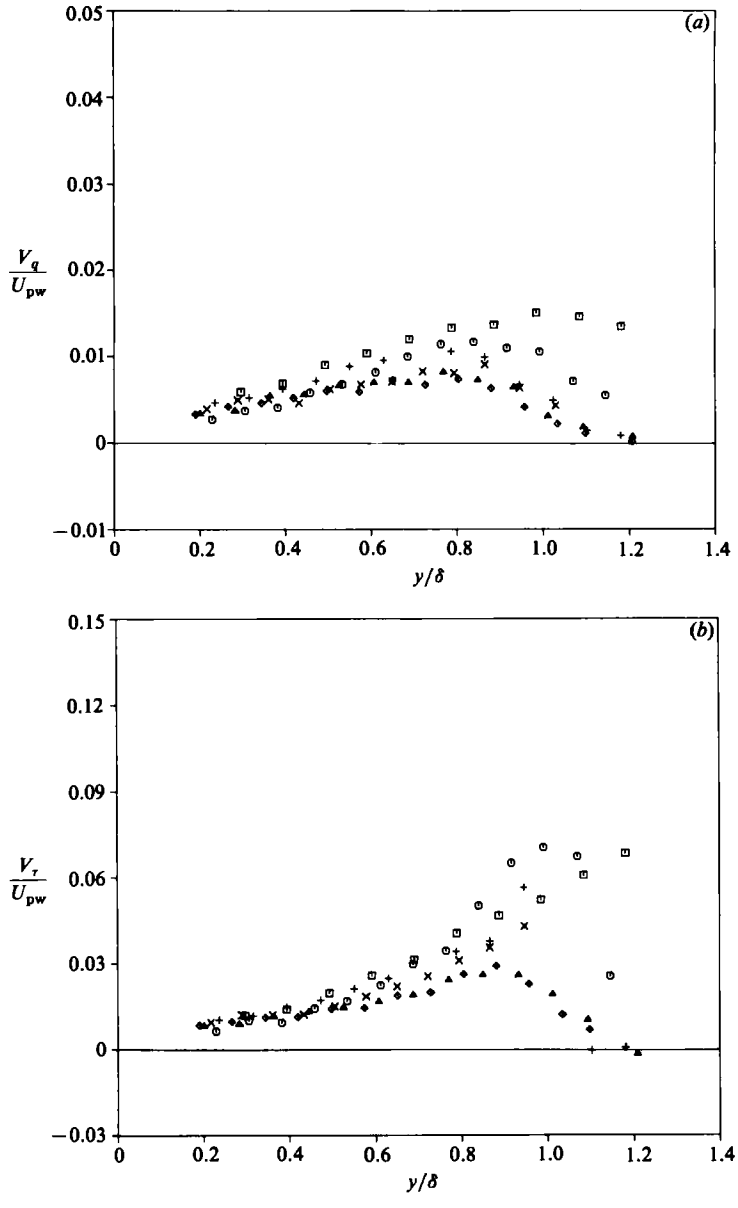

FIGURE 7. Turbulent transport velocities. (*a*) For turbulent kinetic energy V_q/U_{pw}. (*b*) For shear stress, V_τ/U_{pw}.

The triple products of velocity fluctuations are again reduced by convex curvature, by a factor of about 0.5 in mid-layer: in the experiment of Gibson *et al.* the reduction is slightly less and even the flat-surface values are typically 20% higher. The turbulent 'transport' velocities show significantly smaller effects of curvature than the eddy diffusivities. If diffusion by pressure fluctuations is neglected, the transport velocities for turbulent kinetic energy and shear stress can be approximated respectively by $V_q = \overline{q^2 v}/\overline{q^2}$, where $q^2 = u^2+v^2+w^2$, and $V_\tau = \overline{uv^2}/\overline{uv}$. Measurements are shown in figure 7: profiles of individual triple products are given by Muck. The decrease with increasing downstream distance over the main part of the boundary layer is only just significant, in contrast to the eddy diffusivities, which decrease as

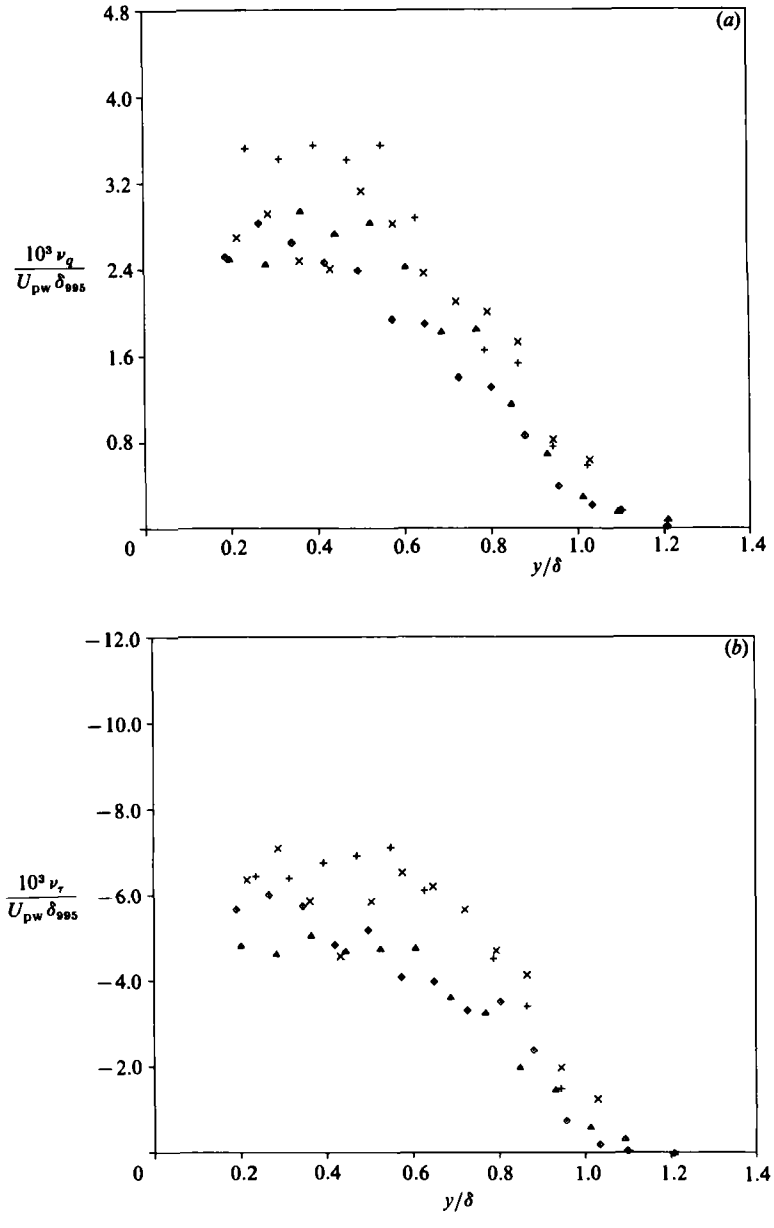

FIGURE 8. Eddy diffusivities. (*a*) For turbulent kinetic energy $10^3\nu_q/(U_{pw}\delta_{995})$. (*b*) For shear stress $10^3\nu_\tau/(U_{pw}\delta_{995})$.

much as the triple products themselves. However, the decreases near the outer edge are large, with a slow start followed by a rapid drop. The decrease in V_τ is particularly significant when one remembers that $\overline{uv}$ itself is attenuated near the outer edge of the boundary layer, both absolutely and in comparison with the mean-square intensity. However, even the large readjustment of shear-stress transport velocity seems to be essentially complete by the third measurement station, about 15 boundary-layer thicknesses from the start of the curvature, and the transport velocity of turbulent kinetic energy seems to react even more rapidly. The u-component

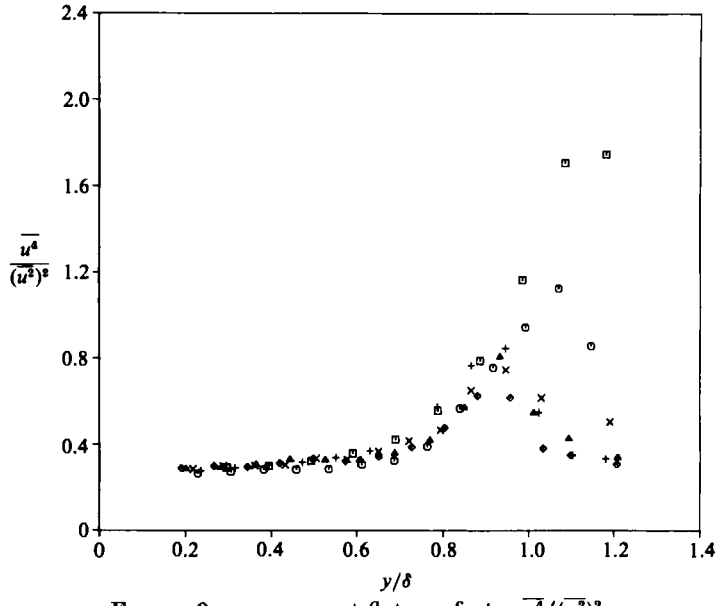

FIGURE 9. u-component flatness factor $\overline{u^4}/(\overline{u^2})^2$.

and v-component skewness factors seem to react to the application of curvature rather more slowly than the transport velocity. The question of which is the more meaningful form of dimensionless triple product depends on the purpose in view, but it is clear that interpretations of flow behaviour should not be based on only one set of parameters.

Figure 8 shows the eddy diffusivities of turbulent energy and of shear stress. Unlike the eddy diffusivity of momentum ('eddy viscosity') these are genuine turbulence parameters, but would be expected to be simply behaved only if all the turbulent eddies were small compared with the width of the flow (corresponding to the usual condition of validity of gradient-diffusion concepts in the kinetic theory of gases that the mean free path shall be small compared with the flow width). The eddy diffusivities seem to be more affected by curvature than the transport velocities shown in figure 7, although the eddy-diffusivity formulation makes the large percentage changes in the outer part of the boundary layer less obvious to the eye. Gibson *et al.* show that the diffusivities of kinetic energy and shear stress scale on $\overline{q^2}\,\overline{v^2}/\epsilon$ even in the curved region. Values given by Gibson *et al.* agree with ours to within 10–15%, more closely than the raw triple products, and the same appears to be true of the transport-velocity data.

The flatness factors of u, v, and w remain close to the Gaussian value of 3 over the inner half of the boundary layer even after the start of curvature, but are strongly reduced by curvature in the outer part of the boundary layer as seen for the u-component flatness in figure 9. Once more, the adjustment seems to be virtually complete by the third measurement station. It will be seen below that the reduction in flatness factor is caused by an increase in the ratio of fluctuation intensity in the irrotational flow to that in the turbulent region, rather than by a change in intermittency (recall that, if irrotational-zone fluctuations are negligible and the probability distribution within the turbulent regions is exactly Gaussian, the flatness factor F is related to the intermittency factor γ by $F = 3/\gamma$).

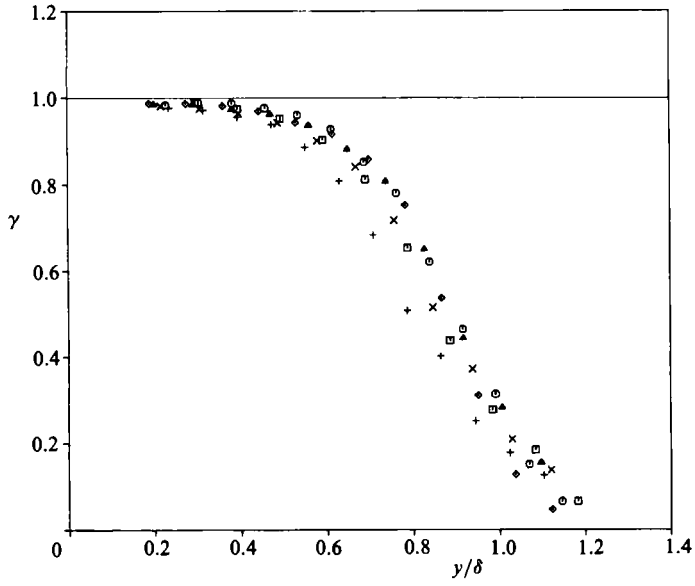

FIGURE 10. Intermittency factor γ.

Figure 10 shows the intermittency factor, deduced from the on–off nature of the temperature-fluctuation records. 'Hot' regions are counted as turbulent and 'cold' regions as irrotational: the ratio of the diffusivity of vorticity to that of heat, i.e. the Prandtl number, is near unity and the Reynolds number is high. There is very little effect of curvature except for $y/\delta > 1$ where the decrease appears to be significant. The lower intermittency at the first measuring station after the onset of curvature was repeatable, and does not seem to arise from inaccurate deduction of δ_{995} from the pseudo-velocity plot as such, but may possibly be due to inadequacy of the simple 'centrifugal' formulae for normal pressure gradient close to the start of curvature, leading to errors in the deduced velocity profile and thus to errors in δ_{995}.

Conditionally sampled mean-velocity components are presented by Muck and will not be shown here: the main feature of interest is that the difference between the irrotational ('cold')-zone V-component mean velocity and the conventional-average V *increases* with increasing distance downstream, although turbulent activity in general is decaying.

The assessment of conditionally sampled turbulence measurements depends on the baseline used for fluctuation measurements. As in previous papers we chose the conventional-average velocities as baselines for the measurement of fluctuations in both the turbulent and the irrotational regions: the more common practice of measuring fluctuations about the average velocity for the zone concerned seems to us to be misguided, because, if the intermittent region consisted of alterations between effectively constant values of velocity in the 'turbulent' and 'irrotational' regions, all the averages so defined would be zero! In fact, a case can be made for measuring – say – turbulent-zone fluctuations with respect to the irrotational-zone average velocity, since the turbulent bursts are indeed excursions from the non-turbulent background flow. Use of conventional-average velocity as a baseline has the great advantage that, for any statistical-average turbulence quantity Q (such as a mean-square intensity), we have the relation

$$Q = \gamma Q_{\mathrm{H}} + (1+\gamma) Q_{\mathrm{C}},$$

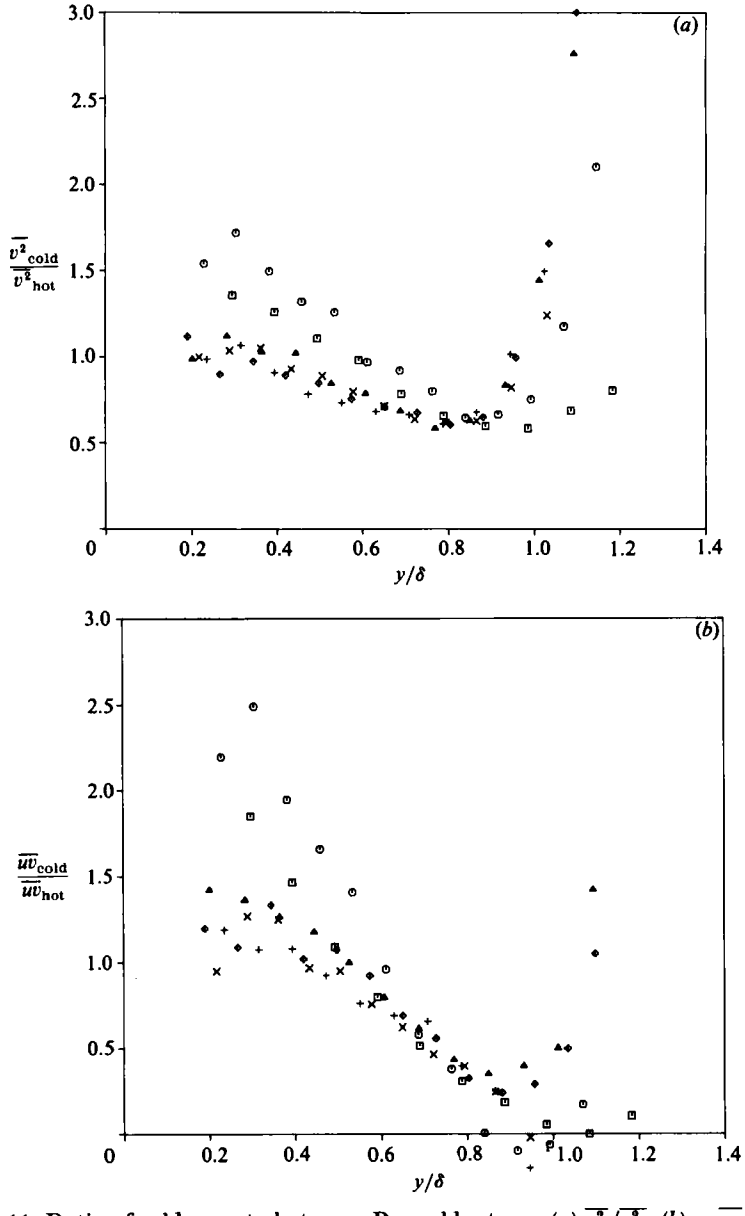

FIGURE 11. Ratio of cold-zone to hot-zone Reynolds stress. (*a*) $\overline{v_{\text{C}}^2}/\overline{v_{\text{H}}^2}$. (*b*) $-\overline{uv}_{\text{C}}/-\overline{uv}_{\text{H}}$.

where Q is the conventional average and Q_{H} and Q_{C} are the turbulent and non-turbulent (irrotational) zonal averages, or the 'hot' and 'cold' zonal averages for short. We refer to the zonal averages multiplied by γ or $(1-\gamma)$ as the zonal 'contributions' to the conventional-average turbulence quantity. Clearly, hot-zone contributions can be deduced from conventional averages and cold-zone contributions, the latter being rather small in cases like the present one: therefore, only cold-zone – i.e. irrotational-zone – contributions to the conventional-average turbulence quantity need to be presented here. The ratios of the cold-zone Reynolds stresses to the hot-zone Reynolds stresses are shown in figure 11. Values for small y may not be trustworthy, because when γ tends to unity even small errors in intermittency determination will

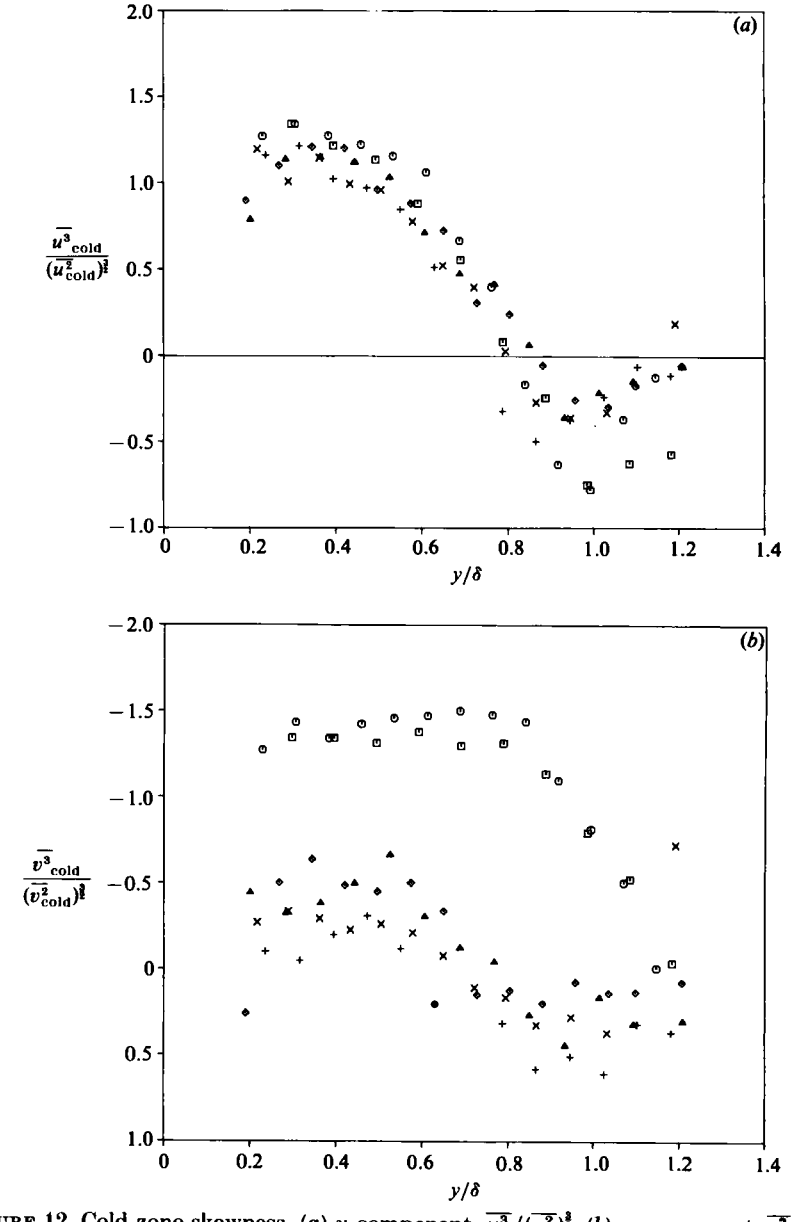

FIGURE 12. Cold-zone skewness. (*a*) u-component, $\overline{u_{\text{C}}^3}/(\overline{u_{\text{C}}^2})^{\frac{3}{2}}$. (*b*) v-component, $\overline{v_{\text{C}}^3}/(\overline{v_{\text{C}}^2})^{\frac{3}{2}}$.

grossly contaminate the cold-zone averages with hot-zone fluid, so that hot-zone and cold-zone averages become equal experimentally if not in truth.

The reduction of the cold-zone contributions to the total Reynolds stresses by curvature is larger than for conventional averages (figure 5) except near the outer edge. The cold-zone contributions to the normal stresses, if not to the shear stress, still seem to be decreasing with increasing x at the last measurement station, in contrast to the conventional-average Reynolds stresses. The *increase* in cold-zone average Reynolds stresses, compared to hot-zone averages, is unmistakable in the outermost part of the layer. The conventional-average velocity is used as a baseline

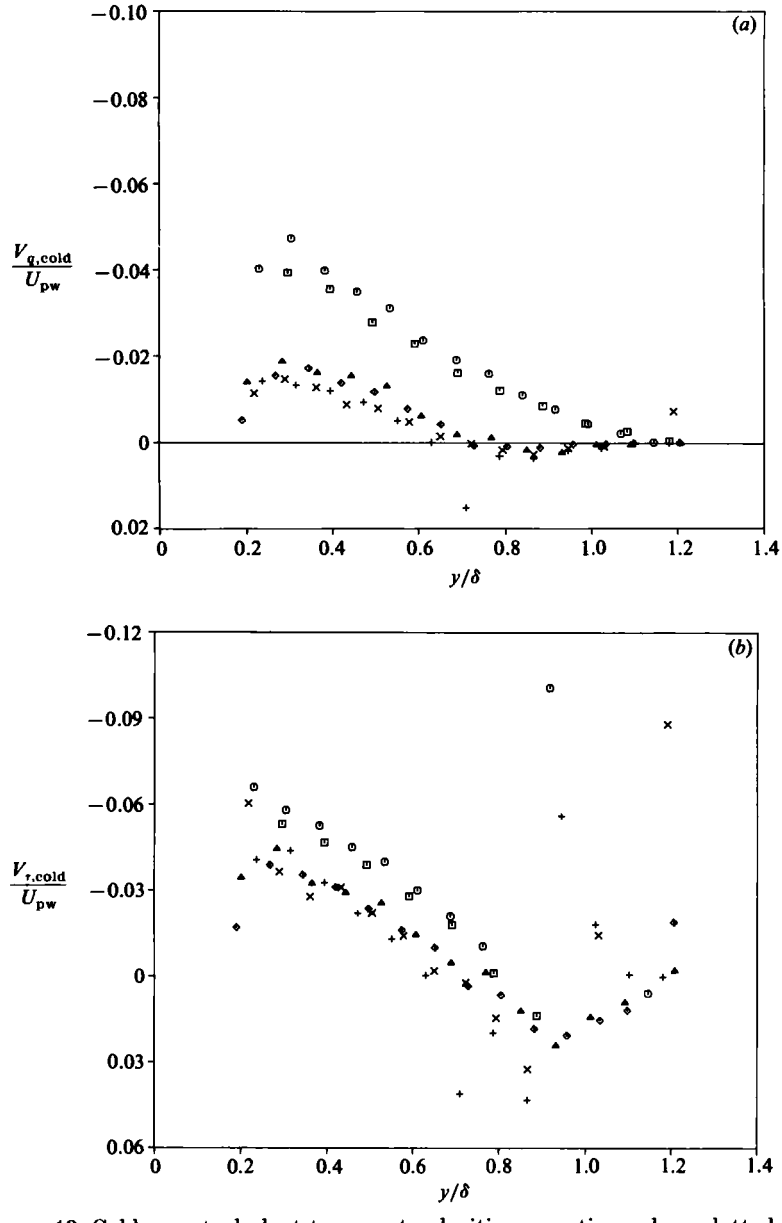

FIGURE 13. Cold-zone turbulent transport velocities; negative values plotted upwards. (*a*) For turbulent kinetic energy $V_{q,\mathrm{C}}/U_{\mathrm{pw}}$. (*b*) For shear stress $V_{\tau,\mathrm{C}}/U_{\mathrm{pw}}$.

for all fluctuations, so that, if the velocity simply alternated between a constant cold-zone value and a (different) constant hot-zone value, then the ratio of mean-square cold-zone fluctuations $\overline{u_{\mathrm{C}}^2}$, say, to the corresponding hot-zone mean-square fluctuation would be simply $\gamma^2/(1-\gamma)^2$. An increase in cold-to-hot ratio, as shown in figure 11, could therefore be caused entirely by an increase in intermittency in the outermost part of the boundary layer, for which there is some slight evidence in figure 10. However, the fractional increases in cold-zone average Reynolds stresses, particularly in $\overline{uv}$, are quite large, and suggest that convex – i.e. stabilizing – curvature

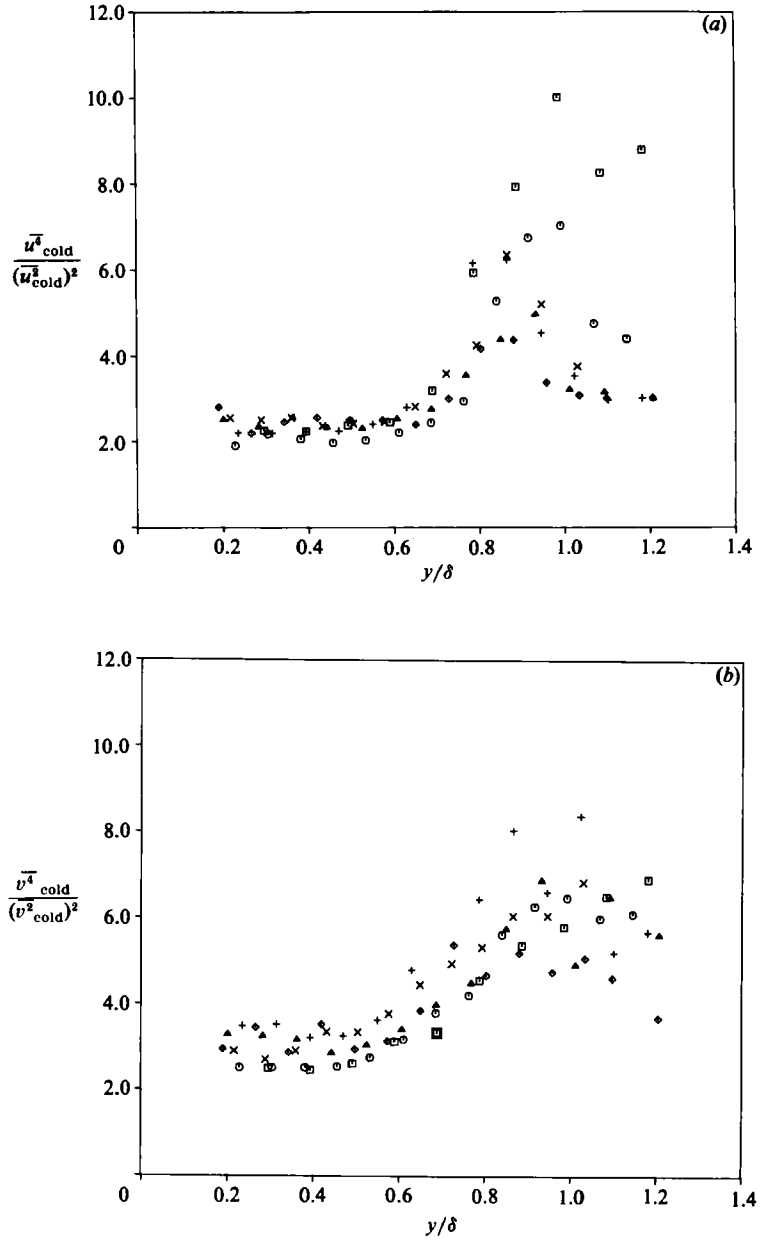

FIGURE 14. Cold-zone flatness factors. (*a*) u-component, $\overline{u_C^4}/(\overline{u_C^2})^2$. (*b*) v-component, $\overline{v_C^4}/(\overline{v_C^2})^2$.

may possibly lead to wave motions in the irrotational region, which may be called 'centrifugal waves' by analogy with the usual term 'gravity waves'. Certainly, the measurements of Castro & Bradshaw (1976) on a stably curved mixing layer showed some evidence for strong, and possibly wave-induced, irrotational fluctuations on the high-velocity side of the mixing layer. Wave-induced fluctuations will not necessarily obey the same modelling laws as (rotational) turbulence, and may therefore confuse modellers if not recognized. However, the effects on conventional-average turbulence parameters are probably negligible at small values of δ/R like those in the present experiment.

The effect of streamline curvature on the cold-zone triple products, shown in figure 12, is somewhat curious. The u-component skewness in the cold zone is very little altered by surface curvature: it falls from the value of $+1$ expected for $\gamma = 1$ according to the above-mentioned 'square-wave' model of turbulence and approaches the conventional average as γ tends to zero. (This is totally different from the behaviour of the conventional-average skewnesses, shown by Muck, which change from small values near the surface to peaks at $y/\delta = 0.9$–1.0 and then tend rapidly to zero: the negative values of cold-zone u-component skewness may possibly be contamination from the negative conventional values, caused by overestimates of the intermittency factor, but are fairly consistent at the different stations.) The cold-zone skewness of the v-component has a value of -1.5 over most of the boundary layer upstream of the region of curvature, falling to nearly zero at the outer edge: a skewness factor of ± 1.5 would be expected in an intermittent process consisting of triangular, rather than square, excursions from the baseline. In the presence of curvature, however, the cold-zone skewness factor of the v-component ranges from about -0.5 near the surface to $+0.5$ in the outer part of the boundary layer, a complete change of behaviour from that found on the flat surface.

The cold-zone transport velocities $V_{q,\mathrm{C}} = (\overline{q^2 v})_{\mathrm{C}}/(\overline{q^2})_{\mathrm{C}}$ and $V_{\tau,\mathrm{C}} = (\overline{uv^2})_{\mathrm{C}}/(\overline{uv})_{\mathrm{C}}$ (figure 13) show, even more markedly than the conventional transport velocities, the usual feature of a rapid decrease from flat-surface values to near-asymptotic curved-surface values by the third measurement station, 390 mm from the start of curvature. The negative values are significant and are the result of transport of irrotational fluid towards the surface by entrainment processes. The difference between irrotational-zone and conventional-mean V-component velocity increases downstream, so the effect just mentioned would be largely hidden (or, strictly, regarded as a mean-flow effect) if the conditional averages were based on zonal-mean velocities as baselines.

The cold-zone flatness factors of u and v (figure 14) are also of some interest. Before the start of curvature, the u-component cold-zone flatness factor is about 2 (compared to the Gaussian value of 3) in the inner half of the boundary layer, rising very considerably in the outer layer: the 'square-wave' model would give a flatness factor of 1.0 everywhere. The large rise in cold-zone flatness factor in the outer part of the boundary layer disappears rather rapidly on the application of curvature, maximum values – in the region $y/\delta \doteq 0.9$ – being only about 5. The v-component cold-zone flatness factor is about 2.5 in the inner half of the boundary layer upstream of the start of curvature, rising to about 6 in the region $y/\delta \doteq 1$: curvature increases this value slightly in the inner part of the boundary layer, while the flatness factor in the outer part of the boundary layer decreases, though less rapidly than for u.

Figure 15 shows the balance of turbulent energy, both upstream of curvature and at the most-downstream station on the convex surface. The pressure-diffusion and dissipation terms were not measured: the former was neglected and the latter was evaluated as the sum of the measured terms to balance the equation. In both cases the production and dissipation rates near the surface are roughly equal to the 'local-equilibrium' values $u_\tau^3/(Ky)$. (Ramaprian & Shivaprasad derived dissipation ϵ from measurements of $\overline{(\partial u/\partial t)^2}$, assuming the dissipating eddies to be isotropic, and their inner-layer values are far from the expected local equilibrium values, requiring implausible values of pressure diffusion to balance the equation.) In the outer part of the boundary layer, production and dissipation rates at given y/δ are, if anything, increased by the application of convex curvature, but it is difficult to say whether the primary effect is on the energy-balance terms as such, or on the relation between true eddy lengthscales and the boundary-layer thickness arbitrarily defined as δ_{995}.

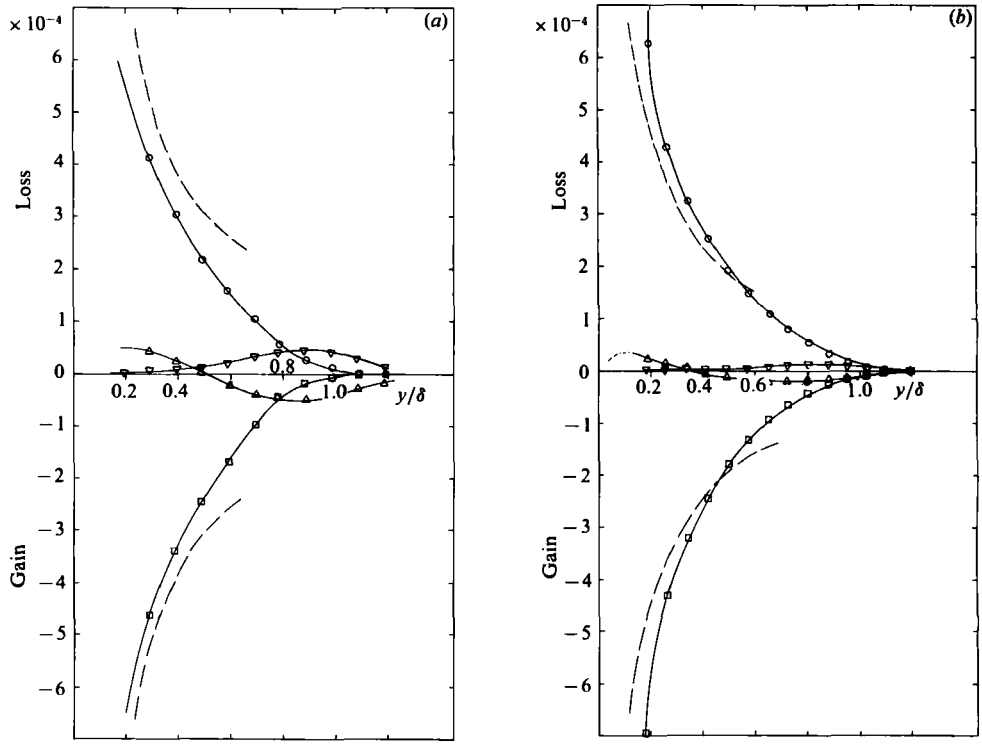

FIGURE 15. Turbulent-kinetic-energy balance: □, production; ○, dissipation; ▽, advection; △, diffusion; ----, $u_\tau^3/(Ky)$. (a) $x = -145$ mm. (b) $x = 1000$ mm.

Undoubtedly, the 'diffusion' (i.e. turbulent transport by triple products and pressure fluctuations) and 'advection' are both considerably decreased by the application of curvature, as would be expected from the above discussion of the behaviour of Reynolds stresses and triple products: clearly, the decrease in Reynolds shear stress and the increase in $\partial U/\partial y$ (see figure 2) have opposing effects on the production rate. Balances of the terms in the shear-stress transport equation are given by Muck, and will not be reproduced here: as usual, the mean and turbulent transport terms in the shear-stress transport equation are quite small compared with the 'generation' term $\overline{v^2}\,\partial U/\partial y$, and, like the corresponding terms in the turbulent-energy equation, become even smaller when convex curvature is applied. The dissipation-length parameter, $L = (-\overline{uv})^{\frac{3}{2}}/\epsilon$, and the corresponding parameter based on the turbulent energy, $L_q = (\overline{q^2})^{\frac{3}{2}}/\epsilon$, were evaluated by Muck for the last convex station only (see figure 18 of II), and both are reduced by about 40% from their flat-surface values, roughly following the behaviour of the mixing length, to which L is equal in local-equilibrium flow.

When the present work was planned, it was expected that important clues to the behaviour of the large-eddy structure would be given by the probability density function of the lengths of the 'hot' (turbulent) and 'cold' (irrotational) zones. In fact the zone-length probability distributions normalized by the boundary-layer thickness are very little affected by curvature and no distinct trend can be identified: quantitative results are given by Muck and, for the more interesting concave case, in II. This null result, and the relatively small changes in the intermittency

distribution after the application of curvature, leads one to believe that the effect of stabilizing streamline curvature on turbulence structures is mainly a quantitative attenuation in intensity rather than a qualitative change in large-eddy configuration.

4. Discussion

The conventional-average Reynolds-stress profiles shown in figure 5 indicate that the response of turbulence to suddenly applied stabilizing streamline curvature is rather rapid, the decrease in turbulence intensity implying a preceding increase in the turbulent-energy dissipation rate, followed by a decrease in dissipation as the flow settles down at the new, lower, level of intensity. The different behaviour of intensity and of dissipation is not paradoxical, because the dissipation rate equals the rate of energy transfer from the larger eddies, and is usually modelled by some expression like $(\overline{q^2})^{\frac{3}{2}}/L_q$ – which simply defines a length L_q but indicates that dissipation depends on some form of turbulence lengthscale as well as on the intensity. A reduction in intensity can still be associated with an increase in ϵ if L_q decreases sufficiently, and both L_q and its distant relative the mixing length do decrease considerably when stabilizing curvature is applied. As the turbulent intensity decreases, the dissipation rate falls again.

In some previous experiments on strongly stabilized curved boundary layers (e.g. So & Mellor 1973; Smits, Young & Bradshaw 1979; Gillis *et al.* 1980; Gillis & Johnston 1983), curvature was sufficiently large to attenuate the normal stresses greatly and to reduce the shear stress almost to zero, in the outer part of the boundary layer. As pointed out by Smits *et al.*, the vanishing of the shear stress in axes which happen to be aligned with the local stream direction is not particularly meaningful: the partition of the stress tensor into normal stresses and shear stresses simply depends on the axes chosen. However, as remarked by Hunt & Joubert (1979), there may be a real distinction between the effects of mild streamline curvature, in which the Reynolds stresses are merely somewhat reduced, and 'strong' curvature in which the Reynolds stresses in the outer part of the boundary layer become negligible, so that what remains is an inner boundary layer – with a non-zero mean shear at its outer edge – topped by a region with significant mean shear but insignificant Reynolds stresses. Smits *et al.* showed, however, that a boundary layer so attenuated by strong curvature recovered rather rapidly, the dimensionless structure parameters like the stress/intensity ratio recovering even more quickly than the absolute intensities. The general conclusion is that convex curvature basically attenuates the existing turbulence structure, perhaps producing significant preferential changes in structure parameters like the stress/intensity ratio, but that significant new types of eddy structure – or significant 'centrifugal-wave' motions – do not appear. One of the motivations of the present work was, was indeed, a search for centrifugal waves, inspired by the evidence of Castro & Bradshaw, but, as mentioned above, we found that quite sensitive measures of large-eddy structure like the intermittency profile and the zone-length statistics were very little altered by stabilizing curvature. The rapid response of boundary layers to suddenly applied stabilizing curvature, and fairly rapid recovery when the curvature is removed, are in strong contrast to the behaviour of boundary layers with concave (destabilizing) curvature as discussed in the companion paper II.

From the point of view of calculation methods, this rapid response to stabilizing curvature is to some extent a simplification since, to a reasonable approximation, structural parameters can be related directly to the local curvature. However, if

structural parameters in lengthscale transport equations (or the equivalent, such as dissipation-rate transport equations) are related directly to local curvature the response times implicit in these equations will be too long. That is, it may be advisable to model the effects of curvature solely in the Reynolds-stress equations, at least partly as a dependence of the 'rapid' part of the pressure–strain redistribution term in the Reynolds-stress transport equation on a suitable dimensionless curvature parameter.

The effects of stabilizing curvature on the triple-product parameters, which appear in the turbulent transport term in the Reynolds-stress transport equations, is somewhat confused. As might be expected, the 'gradient-transport' diffusivities of shear stress and turbulent energy are strongly affected by curvature – though Gibson *et al.* show that they can be scaled as $\overline{q^2}\,\overline{v^2}/\epsilon$ instead of the more usual $(\overline{q^2})^2/\epsilon$. More physically meaningful quantities like the bulk-transport velocities and the skewnesses are affected so little in the present experiment that the change could almost be ignored in calculation methods. However, Smits *et al.* found very large reductions in dimensionless triple products in a strongly curved stabilized boundary layer, and also found that the rate of response or recovery of triple products was much slower than that of the Reynolds stresses (see paper II). The present configuration with $\delta/R \doteq 0.01$ was chosen as representative of real-life flows over turbomachine blades and other highly cambered aerofoils: the large gap between the significant but mild structural changes in the present experiment and the overwhelming changes found in the work of Gillis & Johnston and Smits *et al.* on bend-like flows with $\delta/R = 0.1$ remains to be filled.

5. Conclusions

The main conclusion of this paper and the companion paper II by Hoffmann, Muck & Bradshaw is that the effects of stabilizing and destabilizing curvature on turbulent shear layers are essentially different phenomena. The most obvious evidence is the very rapid response of a boundary layer to the application or removal of stabilizing (convex) curvature, as compared with the slow reaction to concave (destabilizing) curvature. Changes in turbulent-structure parameters on a convex surface, though interesting in detail and important enough to need special attention in turbulence models, are generally not very large (we exclude pseudo-turbulence parameters like mixing length and eddy diffusivity from this statement). The research community in general, and the present authors in particular, have been rather slow in coming to this conclusion, which is strongly hinted at by the totally different processes of laminar-to-turbulent transition on convex and on concave surfaces: in the convex case, the conventional (Tollmien–Schlichting) mode still occurs, perhaps slightly modified, while on concave surfaces the totally different Taylor–Görtler mode appears. Similar conclusions presumably apply to the effects of stabilizing and destabilizing buoyancy, whose limiting cases are a fog and a thunderstorm respectively, although this does not seem to be explicitly recognized by meteorologists who use qualitatively similar, although quantitatively different, correlations for the effects of buoyancy of either sign.

The work of P. H. Hoffmann was supported by the Brown, Boveri Research Center, and we are grateful to Dr M. P. Escudier for advice and encouragement. We are grateful to many colleagues, and in particular to Dr D. H. Wood, for assistance and for helpful discussions.

REFERENCES

CASTRO, I. P. & BRADSHAW, P. 1976 The turbulence structure of a highly curved mixing layer. *J. Fluid Mech.* **73**, 165.

CHRISTIANSEN, T. & BRADSHAW, P. 1981 Effect of turbulence on pressure probes. *J. Phys.* E: *Sci. Instrum.* **14**, 992.

GIBSON, M. M., VERRIOPOULOS, C. A. & VLACHOS, N. S. 1984 Turbulent boundary layer on a mildly curved convex surface. *Expts in Fluids* **2**, 17 and 73.

GILLIS, J. C. & JOHNSTON, J. P. 1983 Turbulent boundary-layer flow and structure on a convex wall and its redevelopment on a flat wall. *J. Fluid Mech.* **135**, 123.

GILLIS, J. C., JOHNSTON, J. P., KAYS, W. M. & MOFFAT, R. J. 1980 Turbulent boundary layer on a convex, curved surface. *NASA CR*-3391 and *Rep. HMT*-31, Thermosciences Divn, Stanford University.

HOFFMANN, P. H., MUCK, K. C. & BRADSHAW, P. 1985 The effect of concave curvature on turbulent boundary layers. *J. Fluid Mech.* **161**, 371.

HUNT, I. A. & JOUBERT, P. N. 1979 Effects of small streamline curvature on turbulent duct flow. *J. Fluid Mech.* **91**, 633.

KLEBANOFF, P. S. 1955 Characteristics of turbulence in a boundary layer with zero pressure gradient. *NACA Rep.* 1247.

KLINE, S. J., CANTWELL, B. J. & LILLEY, G. M. (eds) 1982 In *Proc. 1980–81 AFOSR-HTTM-Stanford Conference on Computation of Complex Turbulent Flows.* Thermosciences Divn, Stanford University.

MERONEY, R. N. & BRADSHAW, P. 1975 Turbulent boundary layer growth over a longitudinally curved surface. *AIAA J.* **13**, 1448.

MUCK, K. C. 1982 Turbulent boundary layers on mildly curved surfaces. Ph.D. thesis, Imperial College, London (available on microfiche from Department of Aeronautics).

RAMAPRIAN, B. R. & SHIVAPRASAD, B. G. 1978 The structure of turbulent boundary layers along mildly curved surfaces. *J. Fluid Mech.* **85**, 273.

SMITS, A. J., YOUNG, S. T. B. & BRADSHAW, P. 1979 The effect of short regions of high surface curvature on turbulent boundary layers. *J. Fluid Mech.* **94**, 209.

SO, R. M. C. & MELLOR, G. L. 1973 Experiments on convex curvature effects in turbulent boundary layers. *J. Fluid Mech.* **60**, 43.

WEIR, A. D., WOOD, D. H. & BRADSHAW, P. 1981 Interacting turbulent shear layers in a plane jet. *J. Fluid Mech.* **107**, 237.